

Deconfinement Transition and Bound States in Frustrated Heisenberg Chains: Regimes of Forced and Spontaneous Dimerization

Weihong Zheng* and Chris J. Hamer**

School of Physics, University of New South Wales, Sydney NSW 2052, Australia

Rajiv R. P. Singh

Department of Physics, University of California, Davis, CA 95616

Simon Trebst[†] and Hartmut Monien

Physikalisches Institut, Universität Bonn, Nußallee 12, 53115 Bonn, Germany

(November 5, 2018)

We use recently developed strong-coupling expansion methods to study the two-particle spectra for the frustrated alternating Heisenberg model, consisting of an alternating nearest neighbor antiferromagnetic exchange and a uniform second neighbor antiferromagnetic exchange. Starting from the limit of weakly coupled dimers, we develop high order series expansions for the effective Hamiltonian in the two-particle subspace. In the limit of a strong applied dimerization, we calculate accurately various properties of singlet and triplet bound states and quintet antibound states. We also develop series expansions for bound state energies in various sectors, which can be extrapolated using standard methods to cases where the external bond-alternation goes to zero. We study the properties of singlet and triplet bound states in the latter limit and suggest a crucial role for the bound states in the unbinding of triplets and deconfinement of spin-half excitations.

PACS Indices: 75.40Gb, 75.10Jm, 75.50Ee

I. INTRODUCTION

In recent years the subject of fractional excitations, or excitations with fractional quantum numbers compared to the non-interacting limit, has attracted considerable attention. Many experiments in high temperature superconducting materials have been interpreted in these terms, and many theories of high temperature superconductors are built around such fractional excitations. However, fractional excitations in a closed system can only arise in groups that have the full quantum numbers of the non-interacting limit. Thus, their unambiguous identification in numerical calculations remains difficult.

In this work we are interested in studying models, where as parameters in the Hamiltonian are varied, one goes from a phase where the excitations have normal quantum numbers to one where they have fractional quantum numbers. We would like to develop series expansion methods by which such transitions can be studied and the onset of fractional excitations can be demonstrated. Although we work with 1D models, the basic methods we develop can be applied in higher dimensions as well.

The best known example of a fractional excitation is a spinon in the spin-half antiferromagnetic Heisenberg chain [1]. It is well-known that the low-lying excitations of this Bethe-ansatz solvable model consist of a two-spinon continuum. Another simple example of a spin-half excitation is a soliton in the Majumdar-Ghosh model [2]. It is a domain-wall which interpolates between the two dimerized ground states of the model. The low-lying excitations, for a closed system, in this case also consist of a soliton-antisoliton continuum [3].

Adding a bond-alternation to the exchange constants of the model leads to confinement of the spin-half excitations. The elementary excitations now become triplets and the spinons or solitons are bound into pairs. In the unfrustrated case, the role of bond-alternation has been studied by mapping onto a massive Thirring model [4]. The frustrated case, where the ground-states are spontaneously dimerized, has been of considerable recent theoretical interest due to its relevance to spin-Peierls systems such as CuGeO_3 . An explicit bond-alternating term in the Hamiltonian can be motivated as a mean-field representation of the inter-chain elastic couplings [5]. Uhrig *et al.* [6] and Affleck and collaborators [7] have studied the confinement transition for the soliton-antisoliton pairs when such a term is added to the Hamiltonian.

Here, we approach these transitions from the opposite direction. We study these systems in a strong-coupling perturbation theory, which begins with the limit of decoupled spin-dimers and treats the inter-dimer couplings as a perturbation. In the limit of weakly coupled dimers, the elementary excitations are triplets, which are weakly

dispersive. In this limit our strong coupling theory is highly accurate and we can find all details of various two-particle bound (and antibound) states. The overall 2-particle spectrum is much richer than that obtained in previous studies. Several singlet and triplet bound states and quintet antibound states are found. The number of bound states depends on the coupling constants as well as the wavevector. We study the binding energy and the coherence length associated with the bound states. We also study the singularity at the critical wavevectors where the binding energy goes to zero and the state merges into the continuum.

Using high order series expansions and extrapolation methods we also study the uniform limit, where the bond-alternation term in the Hamiltonian goes to zero. Thus we approach the limit where the triplet excitations break up and spin-half excitations become deconfined. Series expansion results show that as the bond-alternation term goes to zero in the Hamiltonian, the spectral weights associated with triplet quasiparticles go to zero and the lowest lying singlet and triplet excitations become degenerate. These phenomena provide a remarkably clear and simple confirmation of the existence of free spin-half excitations in this limit.

In the frustrated system, the reorganization of the many-body spectra as the system undergoes the deconfinement transition presents an interesting puzzle. Since there is a gap, Δ , to triplet excitations, the two-triplet continuum begins at 2Δ . Thus, in the confined phase, this continuum is separated from the elementary triplet by a second gap. However, when the spin-half excitations are liberated, the resulting low energy spectrum consists of a soliton-antisoliton continuum, which does not have such a second gap. The consistency of the two pictures requires that in the confined phase, between the elementary triplet and the two-triplet continuum there must be a large number of states, which upon deconfinement turn into the continuum. On general grounds, these states must include 2, 3, 4, \dots , triplet bound states, i.e. states involving an arbitrary number of triplets, which must correspond to a soliton-antisoliton pair with arbitrary separation. We discuss insights from studies of two-particle bound states on this issue.

Another interesting puzzle lies in the spectrum of the Majumdar-Ghosh model ($\delta = 0$, $\alpha = 1/2$) near $k = \pi/2$. For both $S = 0$ and $S = 1$, previous studies [3,8,9] have emphasized a bound state below the soliton-antisoliton ($s - \bar{s}$) continuum. To our knowledge, it has not been noticed that the two triplet continuum (the $s - \bar{s} - s - \bar{s}$ continuum) falls below the soliton-antisoliton continuum around this wavevector. In our numerical study, we find that except for a tiny region very near $k = \pi/2$, the latter continuum also falls below the bound states. This raises questions about the stability of the bound states away from $k = \pi/2$.

Another puzzle in our studies is how the energy levels might cross each other. On general grounds, one might expect that the levels for n -particles with varying n cross each other as the parameters are varied. For small values of the perturbation parameter, the energies are arranged in order of increasing n . However, as one approaches $\lambda = 1$, low energy states from each n -sector may appear even below the two-particle continuum. Since n is not a good quantum number, it is not clear how this will reflect itself in our perturbation theory. This deserves further attention.

The organization of the paper is as follows. In section II, we describe the Hamiltonian studied and the various parametrizations used. In section III, we study the regime of forced or externally imposed dimerization. This is a regime where our series expansions are convergent and we present spectra, binding energies, coherence lengths etc. in great detail. In section IV, we consider the regime of spontaneous dimerization, which requires the use of series extrapolation methods. In section V, we present discussions and conclusions.

II. HAMILTONIAN

We wish to study the alternating Heisenberg chain with frustration [3,7,10-14,8],

$$H = \sum_i [(1 + (-1)^i \delta) \mathbf{S}_i \cdot \mathbf{S}_{i+1} + \alpha \mathbf{S}_i \cdot \mathbf{S}_{i+2}], \quad (1)$$

where the \mathbf{S}_i are spin- $\frac{1}{2}$ operators at site i , α parameterizes a next-nearest neighbor coupling and δ is the alternating dimerization. We rewrite the Hamiltonian as

$$H = (1 + \delta) \sum_i [\mathbf{S}_{2i} \cdot \mathbf{S}_{2i+1} + \lambda (\mathbf{S}_{2i} \cdot \mathbf{S}_{2i-1} + y \mathbf{S}_i \cdot \mathbf{S}_{i+2})], \quad (2)$$

The parameter space (δ, α) is equivalent to the parameter space (λ, y) with $\lambda \equiv (1 - \delta)/(1 + \delta)$ and $y \equiv \alpha/(1 - \delta)$. The latter parametrization makes explicit that for $\lambda = 0$, the model consists of decoupled dimers: we take this to be our unperturbed Hamiltonian H_0 . The rest of the Hamiltonian can be treated as a perturbation, and we can expand various physical quantities in powers of λ . The formalism for studying n -particle sectors in perturbation theory is discussed in detail in a companion paper [15].

The series expansions for the ground state energy and triplet excitation spectrum have previously been computed [11] up to order 23. The two-particle excitations have been discussed using a leading order Brueckner ansatz calculation [13], a second order series expansion [14] and an RPA study [10]. With our new technique, we perform high-order series expansions in powers of λ for fixed values of y [16]. As discussed in a companion paper [15], we first calculate an effective Hamiltonian in the two-particle sector

$$E_2(\mathbf{i}, \mathbf{j}; \mathbf{k}, \mathbf{l}) = \langle \mathbf{k}, \mathbf{l} | H^{\text{eff}} | \mathbf{i}, \mathbf{j} \rangle, \quad (3)$$

and then calculate the irreducible two-particle matrix element

$$\begin{aligned} \Delta_2(\mathbf{i}, \mathbf{j}; \mathbf{k}, \mathbf{l}) = & E_2(\mathbf{i}, \mathbf{j}; \mathbf{k}, \mathbf{l}) - E_0(\delta_{\mathbf{i}, \mathbf{k}}\delta_{\mathbf{j}, \mathbf{l}} + \delta_{\mathbf{i}, \mathbf{l}}\delta_{\mathbf{j}, \mathbf{k}}) - \Delta_1(\mathbf{i}, \mathbf{k})\delta_{\mathbf{j}, \mathbf{l}} - \Delta_1(\mathbf{i}, \mathbf{l})\delta_{\mathbf{j}, \mathbf{k}} \\ & - \Delta_1(\mathbf{j}, \mathbf{k})\delta_{\mathbf{i}, \mathbf{l}} - \Delta_1(\mathbf{j}, \mathbf{l})\delta_{\mathbf{i}, \mathbf{k}}, \end{aligned} \quad (4)$$

where δ refers to a Kronecker delta function and Δ_1 is the one-particle irreducible matrix element.

Here we will only concentrate on the expansions for the following two lines in the parameter space: (i) $\alpha = 0$, corresponding to nearest neighbor interaction only, and (ii) $\alpha = (1 - \delta)/2$, which is a special line in the parameter space where the ground states are known exactly, also known as the Shastry-Sutherland line. The model at $\delta = 0$ ($\lambda = 1$) is the uniform Heisenberg chain in case (i) and the Majumdar-Ghosh model in case (ii).

III. BOUND STATES WITH FORCED DIMERIZATION

In this section we study the small- λ regime, where our strong coupling expansions are convergent. Thus a simple truncation of the relevant power series expansions leads to highly accurate results. We discuss the number of bound states with different quantum numbers as well as their binding energies, the range of k -values where the bound states exist, the coherence length associated with the bound-pair as well as the singularities at the critical wavevector, where the binding energy goes to zero and the bound state merges into the continuum. We first consider the model with $\alpha = 0$ and then $\alpha = (1 - \delta)/2$.

1. Case $\alpha = 0$

For the case without the second neighbor interaction ($\alpha = 0$), the series for the irreducible two-particle matrix element Δ_2 have been computed up to order 7 for singlet bound states, and to order 11 for triplet and quintet states [16]. The reason why the singlet series is computed to only 7th order compared to 11th order for the triplet and quintet states is that the singlet has the same quantum numbers as the ground state. Thus a much more elaborate orthogonalization method is required to implement the cluster expansion [15].

In this model, we find two singlet (S_1 and S_2) and two triplet (T_1 and T_2) bound states below the two-particle continuum, and two quintet antibound states (Q_1 and Q_2) above the continuum. The existence of the second pair of bound states has not been reported by previous calculations, most likely due to a limited precision or a general incapability to deal with multiple bound states. The series for their energies (and also the lower edge and upper edge of the continuum) at band maximum $k = \pi/2$ are given in Table I. Note that there are some discrepancies for the energy of the lowest singlet bound state with the previous second order calculations [13]. Our second order results agree with the series results of Barnes *et al.* [14], but disagree with the results of the Brueckner ansatz calculation [13]. Although the Brueckner ansatz is an expansion of the self-energy in terms of the density of excitations, it normally can recover the first few order of the series expansion in λ exactly: it does give the correct second order result for the triplet bound state. [13]

In the limit $\lambda \rightarrow 0$, the formation of bound/antibound states S_1 , T_1 and Q_1 is well known, due simply to the interaction of two triplets on neighboring sites, and the wave function for S_1 , for example, is

$$|\psi_{S_1}(k)\rangle = \frac{1}{\sqrt{3N}} \sum_j e^{2ik(j+1/2)} [t_1^\dagger(j)t_{-1}^\dagger(j+1) + t_{-1}^\dagger(j)t_1^\dagger(j+1) - t_0^\dagger(j)t_0^\dagger(j+1)]|0\rangle, \quad (5)$$

where $|0\rangle$ is the ground state at $\lambda = 0$ consisting of nonoverlapping spin singlets on each dimer, and $t_\alpha^\dagger(j)$ is a triplet creation operator which excites the singlet at j -th dimer into a triplet state with $S_z = \alpha$, ($\alpha = -1, 0, 1$).

It is interesting also to look at the structure of these new bound states S_2 , T_2 and Q_2 in this limit. To compute their wavefunctions, one needs to diagonalize the second order effective Hamiltonian in the two-particle sector, which

can be reduced to an infinite dimensional symmetric tridiagonal matrix. Our calculations show that in this limit, the bound/antibound states S_2 , T_2 and Q_2 only exist at $k = \pi/2$, and their wave functions are (we take $S_z = 0$ as example)

$$|\psi_{S_2}(k)\rangle = \frac{1}{\sqrt{3N}} \sum_j e^{2ikj} \sum_{n=1}^{\infty} f_n [t_1^\dagger(j-n)t_{-1}^\dagger(j+n) + t_{-1}^\dagger(j-n)t_1^\dagger(j+n) - t_0^\dagger(j-n)t_0^\dagger(j+n)]|0\rangle, \quad (6)$$

$$|\psi_{T_2}(k)\rangle = \frac{1}{\sqrt{2N}} \sum_j e^{2ikj} \sum_{n=1}^{\infty} f_n [t_1^\dagger(j-n)t_{-1}^\dagger(j+n) - t_{-1}^\dagger(j-n)t_1^\dagger(j+n)]|0\rangle, \quad (7)$$

$$|\psi_{Q_2}(k)\rangle = \frac{1}{\sqrt{6N}} \sum_j e^{2ikj} \sum_{n=1}^{\infty} f_n [t_1^\dagger(j-n)t_{-1}^\dagger(j+n) + t_{-1}^\dagger(j-n)t_1^\dagger(j+n) + 2t_0^\dagger(j-n)t_0^\dagger(j+n)]|0\rangle, \quad (8)$$

where the amplitude f_n for two triplets sitting at $j-n$ and $j+n$ (i.e. separated by distance $2n$) is

$$f_n = \begin{cases} -\sqrt{15}(-4)^{-n} & \text{for } S_2 \\ -\sqrt{3}(-2)^{-n} & \text{for } T_2 \\ \sqrt{3}2^{-n} & \text{for } Q_2. \end{cases} \quad (9)$$

Thus the formation of these new bound/antibound states is due to an effective interaction between triplets separated by an odd number of singlet dimers. It appears that S_1 , T_1 and Q_1 are fully “localized” states in this limit, with wavefunctions extending only across a single pair of dimers, whereas the states S_2 , T_2 and Q_2 are “extended”, with the tail of the wavefunctions decreasing exponentially with distance. Our calculations show that at finite λ and for the particular case $k = \pi/2$, the wavefunctions for S_2 , T_2 and Q_2 still only involve triplets separated by an odd number of singlet dimers, while the wavefunctions for S_1 , T_1 and Q_1 only involve triplets separated by an even number of singlet dimers. Thus the spectrum splits into two decoupled sectors at $k = \pi/2$. It would be interesting to explore the dynamics behind this phenomenon in more depth.

With the wavefunction, one can also compute the coherence length L defined by

$$L = \frac{\sum_{d=1}^{\infty} d f_d^2}{\sum_{d=1}^{\infty} f_d^2} \quad (10)$$

where f_d is the amplitude for two triplets separated by distance d . Note that the coherence length L defined here is measured in units of $2a$, where a is the lattice spacing. At the limit $\lambda \rightarrow 0$, $L = 1$ for S_1 and T_1 as expected, while for S_2 and T_2 , L is $32/15$ and $8/3$, respectively.

The two-particle excitation spectrum and the inverse of the coherence length $1/L$ versus momentum k for a rather large dimerization $\delta = 0.6$ are shown in Figs. 1 and 2. One can see that the singlet bound state S_1 exists for the whole range of momenta (its coherence length L is finite also for the whole range of momenta although the coherence length at $k = 0$ is very large, about 6.7706), while other bound/antibound states exist only in a limited range of momenta $k > k_c$. The “critical momentum” k_c for a given bound state can be defined by the inverse of the coherence length $1/L$ tending to zero or by vanishing binding energy. Technically, the first approach may give more reliable results on k_c . The results for the critical momenta k_c versus δ are given in Fig. 3, where we can see that in the limit $\delta \rightarrow 1$, the S_2 , T_2 and Q_2 states exist only at $k = \pi/2$. We can also get the first few terms in the series expansion for k_c for T_1 and Q_1 states. Up to order λ^3 , the dispersions for the T_1 and Q_1 states are

$$E_{T_1}/J(1+\delta) = 2 - \frac{3\lambda}{4} - \frac{9\lambda^2}{32} + \frac{89\lambda^3}{128} + \left(-\frac{\lambda}{2} - \frac{3\lambda^2}{16} + \frac{105\lambda^3}{128} \right) \cos(2k) + \left(\frac{\lambda^2}{4} - \frac{3\lambda^3}{16} \right) \cos(4k) - \frac{37\lambda^3 \cos(6k)}{128} + O(\lambda^4), \quad (11a)$$

$$E_{Q_1}/J(1+\delta) = 2 + \frac{3\lambda}{4} - \frac{\lambda^2}{32} + \frac{21\lambda^3}{128} + \left(\frac{\lambda}{2} - \frac{3\lambda^2}{16} + \frac{37\lambda^3}{128} \right) \cos(2k) + \left(-\frac{\lambda^2}{4} + \frac{13\lambda^3}{64} \right) \cos(4k) + \frac{23\lambda^3 \cos(6k)}{128} + O(\lambda^4). \quad (11b)$$

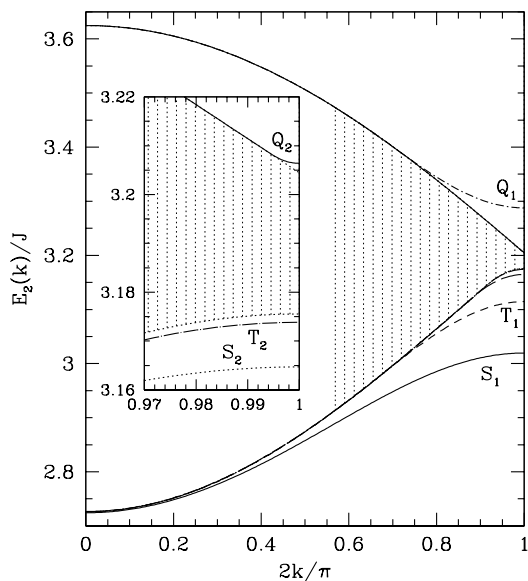


FIG. 1. The excitation spectrum of the $J_1 - J_2 - \delta$ chain with $\delta = 0.6$ and $\alpha = 0$. Beside the two-particle continuum (gray shaded), there are two singlet bound states (S_1 and S_2) and two triplet bound states (T_1 and T_2) below the continuum, and two quintet antibound states (Q_1 and Q_2) above the continuum. The inset enlarges the region near $k = \pi/2$ so we can see S_2 , T_2 and Q_2 below/above the continuum.

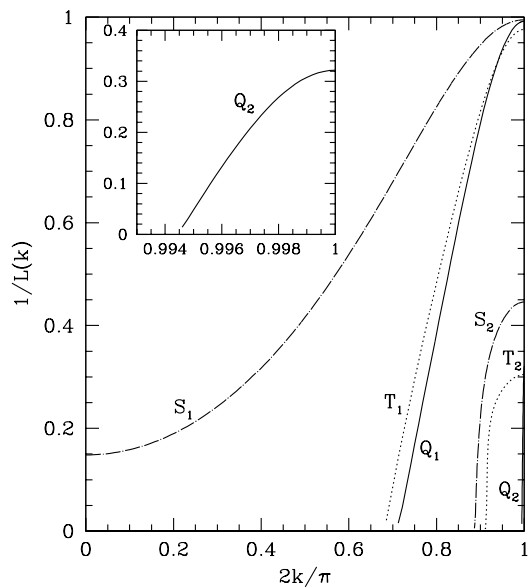


FIG. 2. The inverse of the coherence length $1/L$ versus momentum k for two singlet (S_1 and S_2), two triplet (T_1 and T_2) and two quintet (Q_1 and Q_2) bound/antibound states of the $J_1 - J_2 - \delta$ chain with $\delta = 0.6$ and $\alpha = 0$. The inset enlarges the region near $k = \pi/2$.

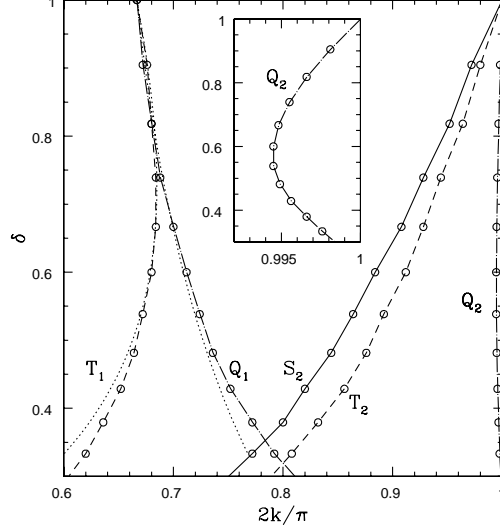


FIG. 3. The critical δ versus momentum k for singlet, triplet and quintet bound/antibound states of the $J_1 - J_2 - \delta$ chain with $\alpha = 0$. The dotted lines are the results of Eq. (12).

With this and the series for the 1-particle triplet excitation spectrum, one can get k_c as

$$2k_c = \begin{cases} 2\pi/3 + 5\lambda/(4\sqrt{3}) - 757\lambda^2/(192\sqrt{3}) + O(\lambda^3) & \text{for } T_1 \\ 2\pi/3 + \sqrt{3}\lambda/4 + 15\sqrt{3}\lambda^2/64 + O(\lambda^3) & \text{for } Q_1 \end{cases} \quad (12)$$

and in the limit $k \rightarrow k_c$, the behaviour of the binding energy is

$$E_b/J\lambda = 4(k - k_c)^2[3/16 - 11\lambda/128 + 591\lambda^2/512 + O(\lambda^3)] + 8(k - k_c)^3[\sqrt{3}/32 + 113x/(256\sqrt{3}) - 25\lambda^2/(768\sqrt{3}) + O(\lambda^3)] + O[(k - k_c)^4] \quad (13)$$

for T_1 , and

$$E_b/J\lambda = 4(k - k_c)^2\left[\frac{3}{16} - \frac{21\lambda}{128} - \frac{39\lambda^2}{256} + O(\lambda^3)\right] + 8\sqrt{3}(k - k_c)^3\left[\frac{1}{32} + \frac{37\lambda}{256} - \frac{37\lambda^2}{1024} + O(\lambda^3)\right] + O[(k - k_c)^4] \quad (14)$$

for Q_1 . Here one can see that the “critical index” for E_b in the limit $k \rightarrow k_c$ is 2, independent of the order of expansion, so one expects that this is *exact*. The results of Eq. (12) are also shown in Fig. 3. We can see that in the limit $\delta \rightarrow 1$, $k_c = \pi/3$ for T_1 and Q_1 , and as δ decreases, k_c for Q_1 increases, while k_c for T_1 firstly increases, then decreases.

Actually S_1 does not always exist in the whole range of momenta: it does not exist at $k = 0$ when $\delta \rightarrow 1$. The inverse of the coherence length L for S_1 at $k = 0$ versus δ is given in Fig. 4, where we can see that as δ approaches 1, L diverges. Because $\lambda = 0$ is a critical point, we cannot get the series directly for the energy gap of S_1 at $k = 0$. We can only get numerical results for it by solving the integral equation [15]. This makes it poorly convergent as $\lambda \rightarrow 1$, as we will see in the next section. In this figure, we also plot the coherence length L at $k = \pi/2$ for S_i and T_i ($i = 1, 2$).

In the limit $\lambda \rightarrow 0$ ($\delta \rightarrow 1$), the binding energy at $k = \pi/2$ for S_1 and T_1 is proportional to λ , as expected, while for S_2 and T_2 , the binding energy is proportional to λ^2 . The rescaled binding energies $E_b/J\lambda^i$ versus δ for S_i and T_i ($i = 1, 2$) are shown in Fig. 5. We also show some numerical exact diagonalization results [14] in this figure, which are in very good agreement with our series results.

As evident from Figs. 4 and 5 the bound state T_2 may disappear at about $\delta = 0.2$.

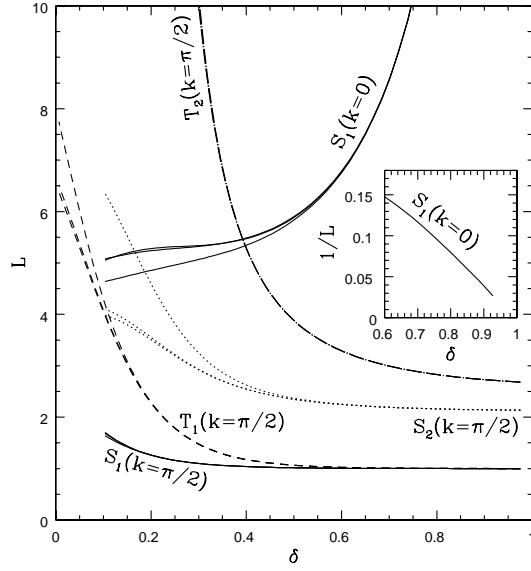


FIG. 4. The coherence length L versus δ for two singlet (S_1 and S_2) and two triplet (T_1 and T_2) bound states of the $J_1 - J_2 - \delta$ chain at $k = 0, \pi/2$ and $\alpha = 0$. The inset plots $1/L$ versus δ for S_1 at $k = 0$. The results of the three highest orders are plotted.

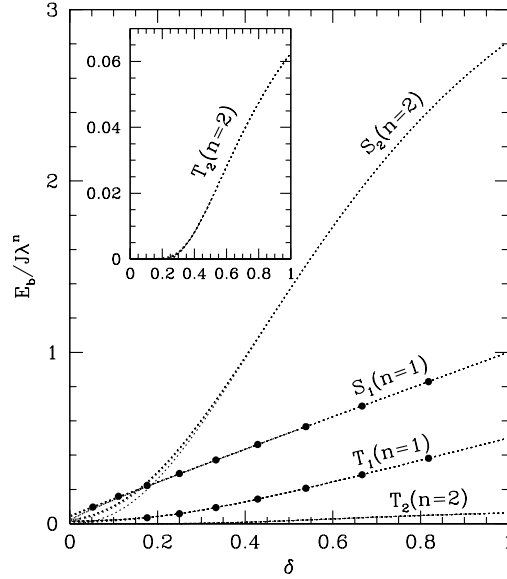


FIG. 5. The scaled binding energy $E_b/J\lambda^n$ at $k = \pi/2$ versus dimerization δ for two singlet (S_1 and S_2) and two triplet (T_1 and T_2) bound states of the $J_1 - J_2 - \delta$ chain with $\alpha = 0$. The solid points are the numerical exact diagonalization results [14]. The inset enlarges the region for T_2 . Several different integrated differential approximants to the series are shown.

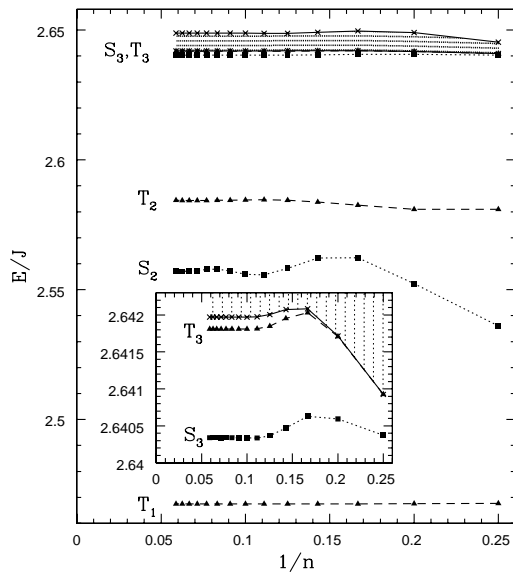


FIG. 6. The energy gap E/J at $k = \pi/2$ for two singlet (S_2 and S_3) and three triplet (T_1 , T_2 and T_3) bound states versus the inverse of order $1/n$ for the $J_1 - J_2 - \delta$ chain with $\delta = 0.4$ and $\alpha = (1 - \delta)/2$. The gray shaded regions are the two-particle continuum. The inset enlarges the region near $k = \pi/2$ so we can see S_3 and T_3 below the continuum.

2. Case $\alpha = (1 - \delta)/2$

Along the special line $\alpha = (1 - \delta)/2$, the ground state is an exact product state, with the spins on each strongly-coupled bond forming a singlet. For non-zero δ , the elementary excitations for this system are triplets. When $\delta \rightarrow 0$, the system has two degenerate ground states and the triplets unbind into a pair of free spin-half excitations. These spin-half objects, which are domain walls between the two ground states, are called solitons and they become the elementary excitations of the system.

The series for the irreducible two-particle matrix element Δ_2 has been computed up to order λ^{19} for 2-particle singlet, triplet and quintet states [16,17] by using both orthogonal transformation (two block method) and similarity transformation methods [15]. Hence one can compute the series directly for the dispersion of the bound states using a degenerate perturbation expansion. It turns out that both transformations give identical series for the dispersion of the bound states, up to the order computed, although the series for the irreducible two-particle matrix elements Δ_2 are different (the basis states are different in the two methods). The energy gap at $k = \pi/2$ for one of the singlet bound states, S_1 , is $1 + 3\delta$ exactly [18,9]. The series for the energy gaps of the other bound states (and also the lower edge of the continuum) at $k = 0$ and $\pi/2$ are given in Table II.

Here we find three singlet (S_1 , S_2 and S_3) and three triplet, (T_1 , T_2 and T_3) bound states below the two-particle continuum, and two quintet antibound states (Q_1 and Q_2) above the continuum. The dispersions for these bound states at $\delta = 0.4$ have been shown in Fig.4 of a preceding Letter [19]. To demonstrate the reliability of our results, we plot in Fig. 6 the energy gap at $\delta = 0.4$ and $k = \pi/2$ for all bound states and the two-particle continuum versus the inverse of the order n up to $n = 19$. The results for S_1 are not plotted, since this case is known exactly. From this figure, we can see that the results are very well converged for $n > 10$. In the limit of $\lambda \rightarrow 0$, the binding energy at $k = \pi/2$ for S_1 and T_1 is proportional to λ , as expected, while for S_2 , T_2 , S_3 and T_3 , the binding energy is proportional to λ^2 , λ^2 , λ^4 , λ^6 respectively, as we can see from Table II.

In the limit $\lambda \rightarrow 0$, the wave functions for S_i and T_i ($i = 1, 2$) are trivial, consisting of two triplets separated by $i - 1$ singlet dimers, while the wave functions at $k = \pi/2$ for S_3 and T_3 are (here again we just take $S_z = 0$ for T_3 as example)

$$|\psi_{S_3}(k)\rangle = \frac{1}{\sqrt{3N}} \sum_j \sum_{n=1}^{\infty} e^{2ik(j+n+1/2)} f_n t_1^\dagger(j) t_{-1}^\dagger(j+2n+1)$$

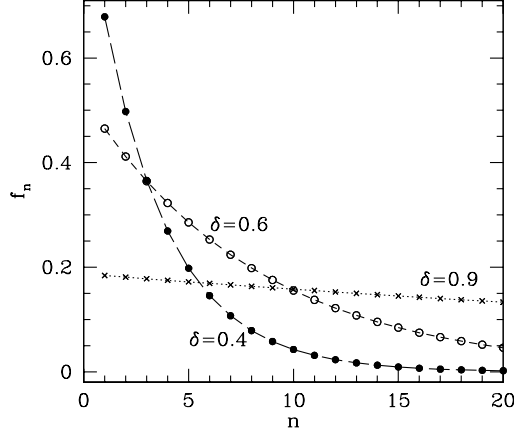


FIG. 7. The amplitude f_n versus n for T_3 with $\delta = 0.4, 0.6$ and 0.9 , and $k = \pi/2$

$$+t_{-1}^\dagger(j)t_1^\dagger(j+2n+1) - t_0^\dagger(j)t_0^\dagger(j+2n+1)]|0\rangle, \quad (15)$$

$$|\psi_{T_3}(k)\rangle = \frac{1}{\sqrt{2N}} \sum_j \sum_{n=1}^{\infty} e^{2ik(j+n+1/2)} f_n [t_1^\dagger(j)t_{-1}^\dagger(j+2n+1) - t_{-1}^\dagger(j)t_1^\dagger(j+2n+1)]|0\rangle. \quad (16)$$

For S_3 , the amplitude f_n for two triplets sitting at j and $j+2n+1$ is

$$f_n = 2^{-n} \sqrt{3}, \quad (17)$$

which decreases by a factor of 2 as n increased by 1. We cannot obtain an analytic expression for f_n for T_3 , but the numerical results for $\delta = 0.4, 0.6$ and 0.9 are presented in Fig. 7: for small λ (large δ), f_n is almost independent of n , so one has an infinite coherence length. From the above results, one can see that the bound states S_3 and T_3 are due to the effective attraction between triplets separated by an even number (exclude 0) of singlet dimers. Thus we find in this case that S_i and T_i ($i = 1, 2$) are fully localized states, whereas S_3 and T_3 are “extended”, with exponential tails to their wave functions. As for the case $\alpha = 0$, our calculations again show that for $k = \pi/2$ and any λ , the wavefunctions for S_2 and T_2 only involve two triplets separated by an odd number of singlet dimers, while wavefunctions for S_1, T_1, S_3 , and T_3 only involve two triplets separated by an odd number of singlet dimers.

The two-particle binding energies and the inverse of the coherence lengths $1/L$ for $\delta = 0.4$ are shown in Figs. 8 and 9. One can see that the singlet bound state S_1 and the triplet bound state T_1 exist for the whole range of momenta, while other bound states exist only in a limited range of momenta $k > k_c$. The results for the critical momenta k versus δ are given in Fig. 10, where one can see that in the limit $\delta \rightarrow 1$, the S_3 and T_3 states exist only at $k = \pi/2$. For S_2 and T_2 bound states, as before, one can get the first few terms in the series expansion for k_c :

$$2k_c = \begin{cases} 2^{1/2}\lambda + 0.53033\lambda^2 + O(\lambda^3) & \text{for } S_2 \\ 2\pi/3 - 7\lambda/(8\sqrt{3}) + 287\lambda^2/(768\sqrt{3}) + O(\lambda^3) & \text{for } T_2 \end{cases} \quad (18)$$

and in the limit $k \rightarrow k_c$, the behaviour of the binding energy is

$$E_b/J\lambda^2 = 4(k - k_c)^2[\lambda^2 + O(\lambda^3)]/32 + 8(k - k_c)^3 \left(\frac{\lambda}{32\sqrt{2}} + 0.107723\lambda^2 + O(\lambda^3) \right) + O[(k - k_c)^4] \quad (19)$$

for S_2 , and

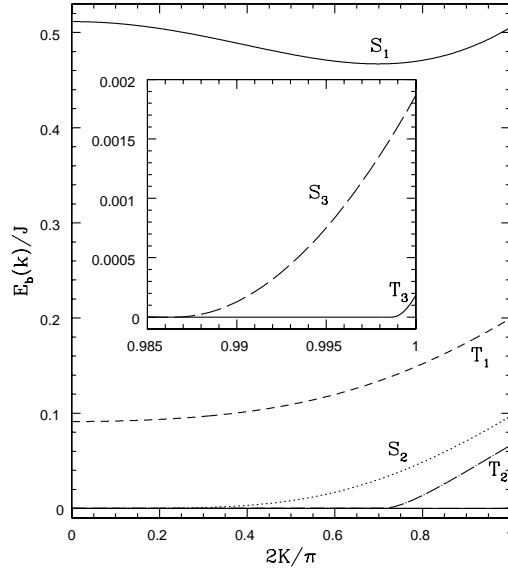


FIG. 8. The binding energy E_b for three singlet (S_1 , S_2 and S_3) and three triplet (T_1 , T_2 and T_3) bound states versus momentum k for the $J_1 - J_2 - \delta$ chain with $\delta = 0.4$ and $\alpha = (1 - \delta)/2$. The inset enlarges the region near $k = \pi/2$ so one can see the nonzero binding energy for S_3 , T_3 .

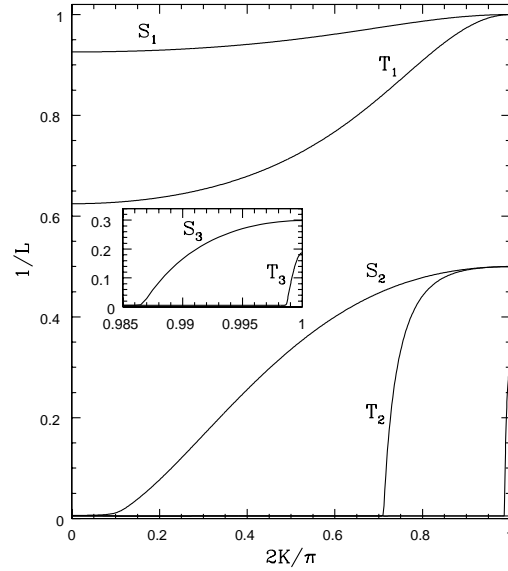


FIG. 9. The inverse of the coherence length $1/L$ versus momentum k for three singlet (S_1 , S_2 and S_3) and three triplet (T_1 , T_2 and T_3) bound states of the $J_1 - J_2 - \delta$ chain with $\delta = 0.4$ and $\alpha = (1 - \delta)/2$. The inset enlarges the region near $k = \pi/2$.

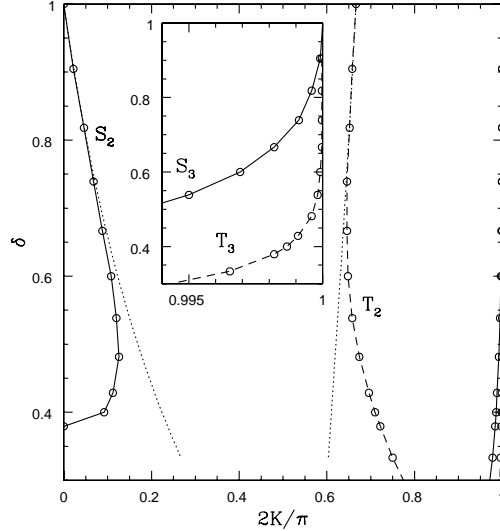


FIG. 10. The critical δ versus momentum k for singlet and triplet bound states of the $J_1 - J_2 - \delta$ chain with $\alpha = (1 - \delta)/2$. The dotted lines are the results of Eq. (18).

$$\begin{aligned}
 E_b/J\lambda^2 = & 4(k - k_c)^2 \left(\frac{3}{32} + \frac{97\lambda}{512} + \frac{461\lambda^2}{1024} + O(\lambda^3) \right) \\
 & + 8(k - k_c)^3 \left(\frac{\sqrt{3}}{64} - \frac{199\lambda}{1024\sqrt{3}} - \frac{19273\lambda^2}{24576\sqrt{3}} + O(\lambda^3) \right) + O[(k - k_c)^4]
 \end{aligned} \quad (20)$$

for T_2 . Here again one can see that the “critical index” is 2. The results of Eq. (18) are also shown in Fig. 10. We can see that in the limit $\delta \rightarrow 1$, $k_c = 0$ and $\pi/3$ for S_2 and T_2 respectively, and as δ decreases, k_c for S_2 firstly increases, then decreases back to 0 at around $\delta = 0.38$, while k_c for T_2 firstly decreases, then increases. We also can see from this figure that S_3 and T_3 only exist over a tiny range of momenta for all δ .

As for S_1 in the case $\alpha = 0$, $\delta \rightarrow 1$ is also a critical point for T_3 at $k = \pi/2$. The inverse of the coherence length L for T_3 at $k = \pi/2$ and S_2 at $k = 0$ versus δ are given in Fig. 11, where we can see that as δ approaches 1, the coherence length for T_3 at $k = \pi/2$ diverges, while the bound state S_2 at $k = 0$ appears at $\delta < 0.38$, consistent with Fig. 10. In this figure, we also plot the coherence length for other bound states at $k = 0$ and $\pi/2$. L is exactly 1 for S_1 at $k = \pi/2$, while for T_1 , S_2 and T_2 at $k = \pi/2$, L is almost equal to 1, 2, 2 respectively for all δ . For S_1 and T_1 at $k = 0$, L is 1 in the limit $\delta \rightarrow 1$, and as δ decreases, L increases. For S_3 at $k = \pi/2$, L is 11/3 in the limit $\delta \rightarrow 1$, and as δ decreases, L decreases.

IV. REGIME OF VANISHING BOND-ALTERNATION: UNBINDING OF SPIN-HALF EXCITATIONS

In this section we turn to the regime of small δ or λ near unity. In this case, our results are less accurate and we have to rely on series extrapolation methods. The limit $\delta \rightarrow 0$ is a critical point, where we expect singularities in various physical quantities. Hence, the convergence of the series breaks down and a simple truncation does not lead to meaningful results. In this case, we use the Dlog Padé and integrated differential approximants [20] to extrapolate the series for the single-particle energies and the two-particle binding energies. We present results based on these extrapolations.

We begin this section by making a few comments about the extrapolation of one and two-particle energies to the $\delta \rightarrow 0$ limit for the nearest neighbor model ($\alpha = 0$). In this case the uniform system at $\delta = 0$ is the Bethe-ansatz solvable nearest-neighbor Heisenberg model, with no gap in the excitation spectrum. Furthermore, it is believed that the mapping on to the massive Thirring model gives the exact spectrum at small k for small δ [10]. The latter

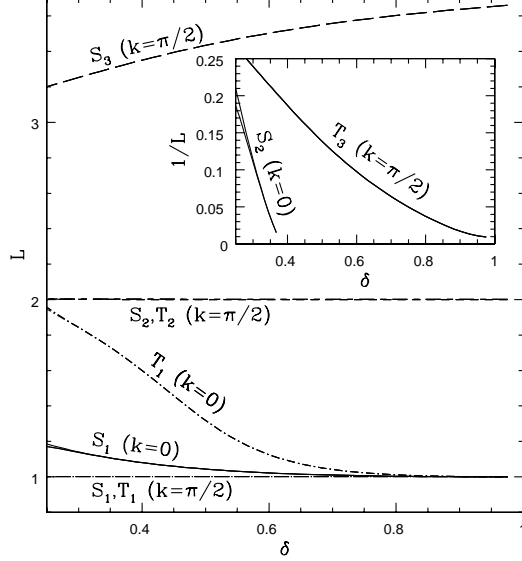


FIG. 11. The coherence length L at $k = 0$ and $\pi/2$ versus δ for three singlet (S_1 , S_2 and S_3) and three triplet (T_1 , T_2 and T_3) bound states of the $J_1 - J_2 - \delta$ chain with $\alpha = (1 - \delta)/2$. The inset plots $1/L$ versus δ for S_2 at $k = 0$ and T_3 at $k = \pi/2$. The results of 17th to 19th order series are plotted.

model has a well defined singlet and a well defined triplet excitation whose energies are in the ratio of $\sqrt{3}$. There are no further bound states so that there are no triplet states between the single particle gap Δ and the two-particle continuum gap 2Δ .

As evident from figures 2, 3, and 4 only one singlet bound state exists as δ goes to zero for $k = 0$. Its coherence length appears large but finite in our calculations, though its binding energy goes to zero. This, together with the elementary triplet whose energy also goes to zero as δ goes to zero, gives the two well defined states expected from the massive Thirring model. As discussed in the previous section, the convergence of the singlet excitation energy at $k = 0$ becomes poor as $\lambda = 1$, as it has to be gotten from a numerical solution of the integral equation rather than from an extrapolation of a binding energy series. This ratio is plotted in Fig. 12. It clearly stays close to 2 down to $\delta = 0.2$ and begins decreasing for smaller values of δ . However, for $\delta < 0.1$ the extrapolations become completely unreliable and we cannot tell if the ratio approaches $\sqrt{3}$ as $\delta \rightarrow 0$.

We now turn to the frustrated model with $\alpha = (1 - \delta)/2$. First, we show the dispersions of the single-particle triplet excitation, the lowest-energy two-particle singlet bound state S_1 , and the bottom of the two-triplet continuum over the full Brillouin zone for various values of δ in Fig. 13. It is evident that the triplet and the singlet spectra become degenerate as δ goes to zero. This is direct evidence for free spin-half excitations, since a pair of free spin-half excitations will form singlet and triplet states of equal energy. Note that previous series expansion studies have shown [11] that the spectral weight associated with the triplets does not vanish over the entire Brillouin zone. It remains finite in the vicinity of $k = \pi/2$ at $\delta = 0$. This result is consistent with the variational calculations of Shastry and Sutherland, [3] who had found a soliton-antisoliton bound state near $k = \pi/2$. Shastry and Sutherland had also found that the bound states were four-fold degenerate meaning that there are degenerate singlet and triplet bound states. Thus, our results are completely consistent with their calculations. Sørensen and collaborators [9] have also given an exact demonstration of triplet and singlet states with energies $(1 + \delta)J$ and $(1 + 3\delta)J$ at $k = \pi/2$ respectively, and thus a splitting of $2\delta J$ which vanishes as $\delta \rightarrow 0$. Our results fit this pattern precisely.

Note further from this figure that as δ goes to zero, in the region not too far from $k = \pi/2$, the two-triplet continuum falls below the states S_1 and E_1 (where E_1 is the single-particle triplet excitation). This is also true for the variational calculation of Shastry and Sutherland shown in Fig. 13(d), though, to our knowledge, it has not been noted before. At $k = \pi/2$, stable singlet and triplet states are rigorously known to exist. A plausible picture is that a stable state exists only at or very near this wavevector, and even at this point its binding energy with respect to the multiparticle continuum is extremely small. It is also likely that the spectral weight of these states is only appreciable in this narrow region; further from $k = \pi/2$, these states will be lost in the continuum, and their spectral weight will be negligible, in

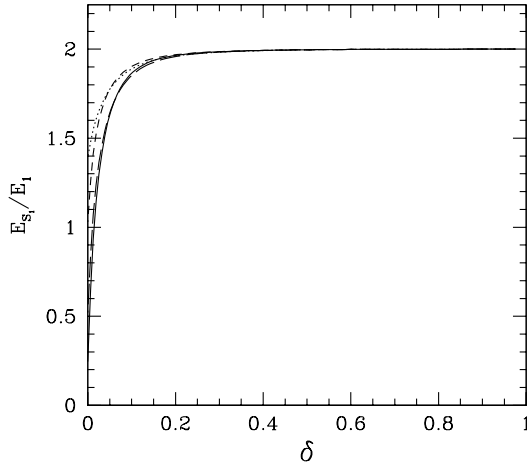


FIG. 12. Ratio of the lowest singlet excitation energy E_{S_1} to the lowest triplet excitation E_1 , in the nearest neighbor model as a function of δ . Results at order 4 (dotted line), 5 (short dashed line), 6 (long dashed line) and 7 (solid line) are plotted.

agreement with the calculation of Singh and Zheng [11].

In the series extrapolation for the figure above, we have made use of the fact that as δ goes to zero (or λ goes to 1), the energy gap approaches a constant with correction proportional to $(1 - \lambda)^{2/3}$ [8], so in the series extrapolation we transform the series to a new variable

$$\lambda' = 1 - (1 - \lambda)^{2/3} \quad (21)$$

to remove the singularity at $\lambda = 1$. Byrnes *et al.* [8] also predict that the singlet-triplet splitting in the limit $\delta \rightarrow 0$ is

$$(E_{S_1} - E_1)/J = c_1\delta + c_2\delta^{5/3}. \quad (22)$$

Our series analysis seem to favor these arguments, as can be seen from Fig. 14. But our results give $c_1 = 2.25(5)$, rather than $15/8$ as given by Byrnes *et al.* [8]; this difference is probably because we choose $\alpha = (1 - \delta)/2$, while in the calculations by Byrnes *et al.* α is fixed to be $1/2$.

In Fig. 15 the binding energy for the lowest triplet bound state T_1 is shown. It is clear that the extrapolation for T_1 does not converge very well. Looking at the figure, it is plausible to suggest that as δ goes to zero the triplet binding energy also approaches $\Delta \approx 0.24J$, the single particle energy gap. If true, this implies that this state also becomes degenerate with the single particle state in this limit. This is consistent with the idea that there are an infinite number of states between the single particle gap Δ and the two-particle continuum, which begins at 2Δ . Thus the lowest of these states must approach Δ in energy. However, we do not see a large number of two-particle bound states in our calculations. We suspect that the other bound states may arise from 3, 4, 5, ..., particle states. We hope to extend our methods to study such multiparticle bound states in the future.

We now turn to the bound states at $k = \pi/2$. We show the rescaled singlet and triplet binding energies at $k = \pi/2$ in Figs. 16 and 17. These results for S_i ($i = 1, 2, 3$) and T_i ($i = 1, 2$) are obtained from the integrated differential approximants to the series, while the results for T_3 are obtained from the numerical solution of the integral equation [15] at orders 14 to 19, since we cannot get the series directly for T_3 . We can see from these figures that as $\delta \rightarrow 0$, the binding energies for all S_i ($i = 1, 2, 3$) approach the same value, which is close to or equal to zero. Among T_i ($i = 1, 2, 3$), T_1 has the largest binding energy in the limit $\delta \rightarrow 1$, but at $\delta = 0.092(3)$, the binding energy for T_1 becomes zero, while the binding energies for T_2 and T_3 are still nonzero, i.e., there appears to be a level crossing between T_i ($i = 1, 2, 3$) here: the level crossing between T_1 and T_2 happens at $\delta = 0.221(1)$ where the binding energy is $E_b/J = 0.11955(10)$. The reason that T_1 and T_2 can cross smoothly is presumably that the bound state for T_1 only involves two triplets separated by an even number of singlet dimers, while the bound state for T_2 only involves two triplets separated by an odd number of singlet dimers, so that the two states lie in disjoint sectors.

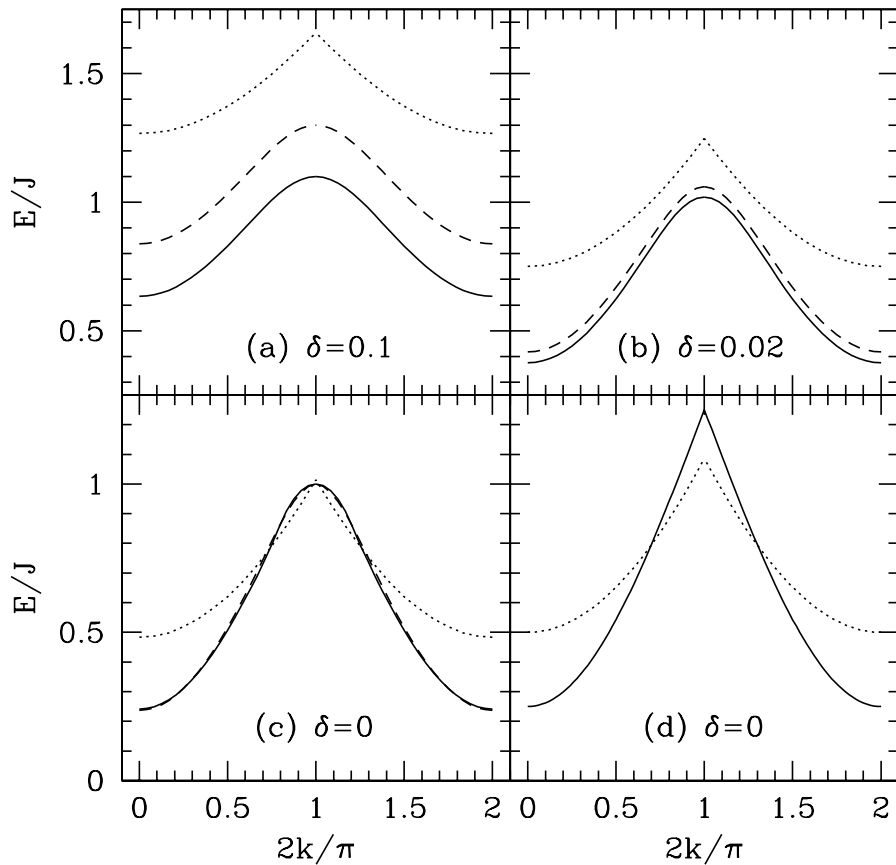


FIG. 13. Dispersion of the single-particle triplet excitation E_1 (solid line), the lowest two-particle singlet bound state S_1 (dashed line), and the bottom of the two-triplet continua (dotted line) for $\delta = 0.1$ (a), 0.02 (b) and 0 (c) for the Shastry-Sutherland model. Window (d) gives the variational results of Shastry and Sutherland, where only the continua are shown.

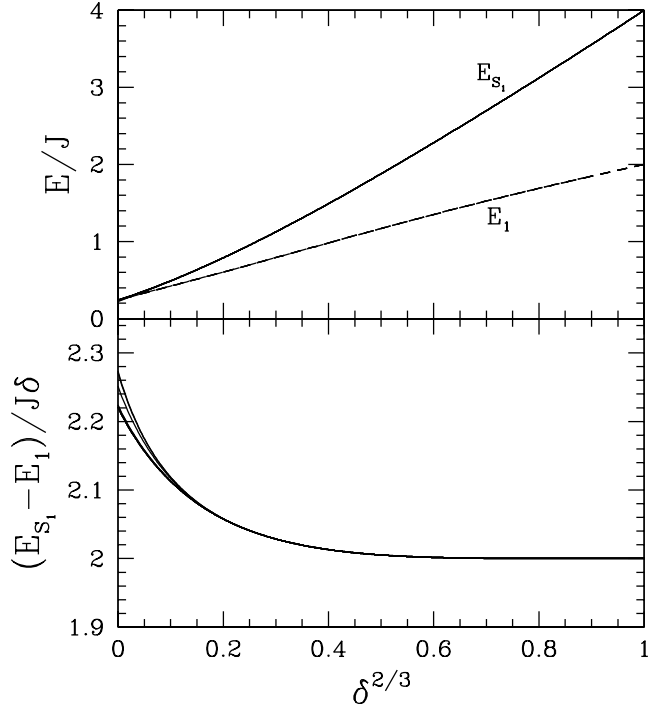


FIG. 14. The 1-particle triplet gap (E_1) and lowest singlet energy gap E_{S_1} at $k = 0$ (upper window), and $(E_{S_1} - E_1)/J\delta$ (lower window) versus $\delta^{2/3}$ for the $J_1 - J_2 - \delta$ chain with $\alpha = (1 - \delta)/2$. The results of several different integrated differential approximants to the series are shown.

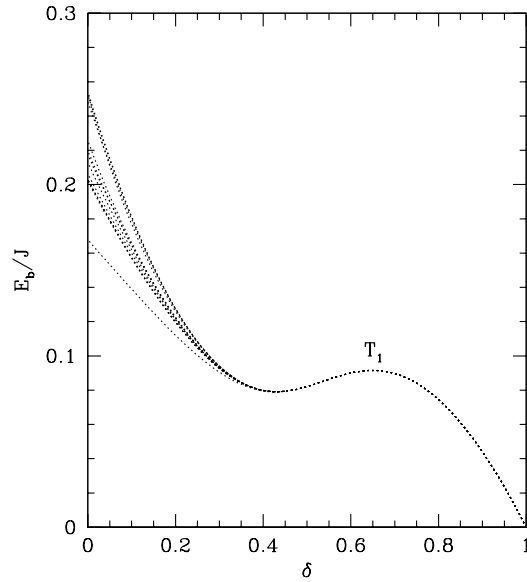


FIG. 15. The binding energy E_b/J of the lowest triplet bound state (T_1) at $k = 0$ as a function of δ . The results of several different integrated differential approximants to the series are shown.

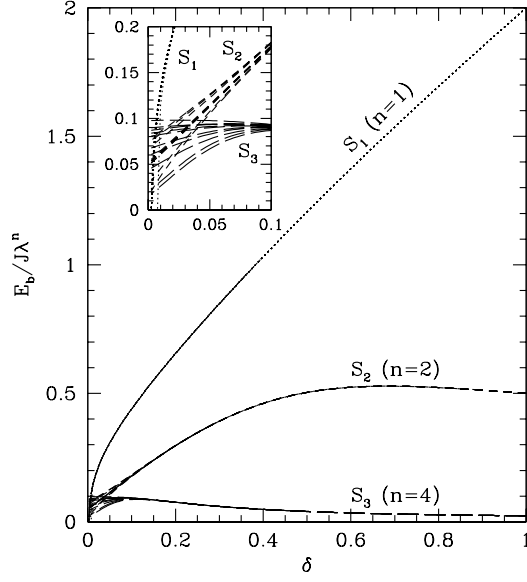


FIG. 16. The rescaled binding energy $E_b/J\lambda^n$ at $k = \pi/2$ versus dimerization δ for three singlet bound states S_i ($i = 1, 2, 3$) of the $J_1 - J_2 - \delta$ chain with $\alpha = (1 - \delta)/2$. The inset enlarges the region near $\delta = 0$. Several different integrated differential approximants to the series are shown.

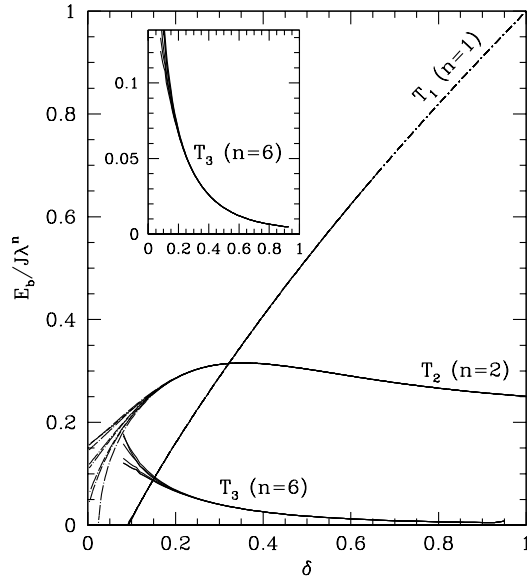


FIG. 17. The rescaled binding energy $E_b/J\lambda^n$ at $k = \pi/2$ versus dimerization δ for three triplet bound states T_i ($i = 1, 2, 3$) of the $J_1 - J_2 - \delta$ chain with $\alpha = (1 - \delta)/2$. The inset enlarges the region for T_3 . For T_1 and T_2 , the results of several different integrated differential approximants to the series are shown, while for T_3 the numerical results from the integral equation at order 14 to 19 are shown.

V. CONCLUSION AND DISCUSSION

In this paper we have carried out an extensive investigation of the two-particle spectra of the frustrated alternating Heisenberg chains using strong coupling series expansions.

In the regime of weakly coupled dimers, the elementary excitations of the system are triplets and the spin-half excitations are confined. In this regime our series expansions are convergent, and we have studied in great detail the properties of the two-particle spectra, including binding energies, coherence lengths and critical properties associated with vanishing binding energies and diverging coherence lengths. We find in every case, just as for the spin ladder system [15], that where a 2-particle bound state emerges below the continuum at a “critical momentum” k_c , the binding energy behaves like $(k - k_c)^2$ as $k \rightarrow k_{c+}$, and the coherence length diverges, as one would expect. Several distinct bound states can be identified, particularly near $k = \pi/2$. Many of the bound states can only be seen by going to sufficiently high orders in the perturbation expansion, showing the extended character of the pair-attraction.

We have also studied the regime of deconfined spin-half excitations ($\delta \rightarrow 0$) by using series extrapolation methods. Several properties of one and two-particle spectra give a clear indication of this deconfinement transition. The spectral weights of the triplets vanish at the transition (except near $k = \pi/2$) and the singlet and triplet excitations become degenerate. These methods can be used to look for such unbinding transitions in higher dimensional models as well.

Our studies also raise several puzzles that need to be addressed in the future. How does the spectrum between Δ and 2Δ get filled up as one goes from the confined to the deconfined phase? We suspect that multi-particle bound states, with varying number of triplets are important. This needs to be further addressed. The picture is much clearer in the soliton language, as one might expect: at small δ , there is a discrete spectrum of $s - \bar{s}$ bound states confined by a linear potential, which becomes continuous as $\delta \rightarrow 0$ and the confining potential vanishes [5,6,8]. Another puzzle is the crossing of energy levels. As λ goes from zero to unity along the Shastry-Sutherland line, one expects to see crossing of n -particle states, with different n . How does this take place? How can this be accounted for within the perturbation theory? Finally, are the Shastry-Sutherland bound states stable away from $k = \pi/2$, where they might decay into the 4-soliton continuum? We hope to address some of these issues in future.

ACKNOWLEDGMENTS

This work was initiated at the Quantum Magnetism program at the ITP at UC Santa Barbara which is supported by US National Science Foundation grant PHY94-07194. The work of ZW and CJH was supported by a grant from the Australian Research Council: they thank the New South Wales Centre for Parallel Computing for facilities and assistance with the calculations. RRPS is supported in part by NSF grant number DMR-9986948. ST gratefully acknowledges support by the German National Merit Foundation and Bell Labs, Lucent Technologies. HM wishes to thank the Yukawa Institute for Theoretical Physics for hospitality. ZW and CJH would like to thank Prof. Oleg Sushkov for some very useful discussions.

* Email address: w.zheng@unsw.edu.au

** Email address: c.hamer@unsw.edu.au

† Present address: Bell Labs, Lucent Technologies, Murray Hill, NJ 07974

- [1] L. D. Faddeev and L. A. Takhtajan, Phys. Lett. A, 375 (1981).
- [2] C.K. Majumdar and D.K. Ghosh, J. Math. Phys. **10**, 1399(1969); C.K. Majumdar, J. Phys. C**3**, 911(1970); P.M. van den Brook, Phys. Lett. **77A**, 261(1980).
- [3] B. S. Shastry and B. Sutherland, Phys. Rev. Lett. **47**, 964 (1981).
- [4] F. D. M. Haldane, Phys. Rev. B **25**, 4925 (1982).
- [5] I. Affleck, in *Dynamical Properties of Unconventional Magnetic Systems* (NATO ASI, Geilo, Norway, 1997).
- [6] G. S. Uhrig and F. Schönfeld, M. Laukamp and E. Dagotto, Eur. Phys. J. B **7**, 67 (1999).
- [7] E.S. Sørensen, I. Affleck, D. Augier and D. Poilblanc, Phys. Rev. B**58**, R14701 (1998).
- [8] T. M. Byrnes, M. T. Murphy, and O. P. Sushkov, Phys. Rev. B**60**, 4057(1999), the second term in Eq. 22 is from private communication with O. P. Sushkov.
- [9] E.S. Sørensen, I. Affleck, D. Augier and D. Poilblanc, in *Density Matrix Renormalization*, edited by I. Peschel, K. Hallberg, and X. Wang, Springer Lecture Notes (Springer, Berlin, 1999).

- [10] G. S. Uhrig and H. J. Schulz, Phys. Rev. B **54**, 9624 (1996).
- [11] R. R. P. Singh and W. H. Zheng, Phys. Rev. B **59**, 9911 (1999).
- [12] G. Bouzerar, A. P. Kampf and G. I. Japardize, Phys. Rev. B **58**, 3117 (1998).
- [13] P. V. Shevchenko, V. N. Kotov, and O. P. Sushkov, Phys. Rev. B **60**, 3305 (1999).
- [14] T. Barnes, J. Riera and D. A. Tennant, Phys. Rev. B **59**, 11384(1999).
- [15] W. H. Zheng, C. J. Hamer, R. R. P. Singh, S. Trebst, and H. Monien, cond-mat/0010354, to be published.
- [16] Explicit results for the series will be made available electronically at <http://www.phys.unsw.edu.au/~zwh>.
- [17] Each series took about 1.5 hours CPU time and about 700MB memory on a Silicon Graphics Power Challenge with a 195MHz R10000 processor.
- [18] W.J. Caspers and W. Magnus, Phys. Lett. **88A**, 103(1982).
- [19] S. Trebst, H. Monien, C. J. Hamer, W. H. Zheng and R. R. P. Singh, cond-mat/0007192, to appear in Phys. Rev. Lett.
- [20] A. J. Guttmann, in *Phase Transitions and Critical Phenomena*, edited by C. Domb and M. S. Green (Academic, New York, 1989), Vol. 13.

TABLE I. Series coefficients for dimer expansions of the energy gap $E/J(1 + \delta)$ of two singlet bound states (S_1 and S_2), two triplet bound states (T_1 and T_2), two quintet antibound states (Q_1 and Q_2), and the lower edge and upper edge of the continuum (C_l and C_u) at $k = \pi/2$ for the $J_1 - J_2 - \delta$ chain with $\alpha = 0$. Nonzero coefficients λ^n up to order $n = 11$ are listed.

n	$E_{S_1}/J(1 + \delta)$ for S_1	$E_{S_2}/J(1 + \delta)$ for S_2	$E_{T_1}/J(1 + \delta)$ for T_1	$E_{T_2}/J(1 + \delta)$ for T_2
0	2.000000000	2.000000000	2.000000000	2.000000000
1	$-5.000000000 \times 10^{-1}$	0.000000000	$-2.500000000 \times 10^{-1}$	0.000000000
2	$1.875000000 \times 10^{-1}$	$-3.906250000 \times 10^{-1}$	$1.562500000 \times 10^{-1}$	$-2.812500000 \times 10^{-1}$
3	$3.906250000 \times 10^{-2}$	$7.812500000 \times 10^{-2}$	$-2.343750000 \times 10^{-2}$	$6.250000000 \times 10^{-2}$
4	$-2.050781250 \times 10^{-2}$	$3.324584961 \times 10^{-1}$	$-6.168619792 \times 10^{-2}$	$9.326171875 \times 10^{-2}$
5	$-4.154459635 \times 10^{-2}$	$-5.464426676 \times 10^{-2}$	$-8.189561632 \times 10^{-2}$	$-1.143256293 \times 10^{-1}$
6	$-4.004075792 \times 10^{-2}$	$-4.499045478 \times 10^{-1}$	$-9.442308214 \times 10^{-2}$	$-1.716450585 \times 10^{-1}$
7	$-2.573965214 \times 10^{-2}$	$-1.200470705 \times 10^{-1}$	$-8.740929615 \times 10^{-2}$	$-2.332303701 \times 10^{-2}$
8			$-6.322668408 \times 10^{-2}$	$2.681890517 \times 10^{-2}$
9			$-2.250317901 \times 10^{-2}$	$-3.523763254 \times 10^{-2}$
10			$2.941323970 \times 10^{-2}$	$1.450322827 \times 10^{-2}$
11			$9.059538250 \times 10^{-2}$	$1.467690427 \times 10^{-1}$
n	$E_{Q_2}/J(1 + \delta)$ for Q_2	$E_{Q_1}/J(1 + \delta)$ for Q_1	$E_{C_l}/J(1 + \delta)$ for C_l	$E_{C_u}/J(1 + \delta)$ for C_u
0	2.000000000	2.000000000	2.000000000	2.000000000
1	0.000000000	$2.500000000 \times 10^{-1}$	0.000000000	0.000000000
2	$3.125000000 \times 10^{-2}$	$-9.375000000 \times 10^{-2}$	$-2.500000000 \times 10^{-1}$	0.000000000
3	$1.250000000 \times 10^{-1}$	$-1.015625000 \times 10^{-1}$	$3.125000000 \times 10^{-2}$	$1.562500000 \times 10^{-1}$
4	$1.513671875 \times 10^{-2}$	$-5.126953125 \times 10^{-2}$	$-2.343750000 \times 10^{-2}$	$9.375000000 \times 10^{-2}$
5	$1.916503906 \times 10^{-2}$	$-1.114908854 \times 10^{-2}$	$-6.868489583 \times 10^{-2}$	$-7.269965278 \times 10^{-3}$
6	$5.786874559 \times 10^{-2}$	$-6.629096137 \times 10^{-4}$	$4.757351345 \times 10^{-3}$	$-1.196628147 \times 10^{-2}$
7	$2.270891195 \times 10^{-2}$	$1.044698998 \times 10^{-2}$	$-1.730789373 \times 10^{-3}$	$8.809831407 \times 10^{-3}$
8	$1.947733239 \times 10^{-2}$	$2.007299524 \times 10^{-2}$	$-3.478056560 \times 10^{-2}$	$4.201953303 \times 10^{-3}$
9	$2.277670953 \times 10^{-2}$	$3.177196538 \times 10^{-2}$	$2.936064788 \times 10^{-4}$	$-2.457848151 \times 10^{-3}$
10	$-1.225328947 \times 10^{-3}$	$4.251490921 \times 10^{-2}$	$5.560815615 \times 10^{-3}$	$8.842688260 \times 10^{-4}$
11	$-9.435317910 \times 10^{-3}$	$5.454945223 \times 10^{-2}$	$-2.004222569 \times 10^{-2}$	$2.355556912 \times 10^{-3}$

TABLE II. Series coefficients for dimer expansions of the energy gap $E/J(1 + \delta)$ of singlet bound states (S_1, S_2, S_3), triplet bound states (T_1 and T_2) and the lower edge of the continuum (C_i) at $k = 0$ and $\pi/2$ for the $J_1 - J_2 - \delta$ chain with $\alpha = (1 - \delta)/2$. Nonzero coefficients of λ^n up to order $n = 19$ are listed.

n	S_1 at $k = 0$	T_1 at $k = 0$	C_1 at $k = 0$	S_2 at $k = \pi/2$
0	2.000000000	2.000000000	2.000000000	2.000000000
1	-1.000000000	-5.000000000 $\times 10^{-1}$	0.000000000	0.000000000
2	-5.000000000 $\times 10^{-1}$	1.250000000 $\times 10^{-1}$	-1.000000000	-7.500000000 $\times 10^{-1}$
3	-2.500000000 $\times 10^{-1}$	-1.562500000 $\times 10^{-1}$	-5.000000000 $\times 10^{-1}$	-6.250000000 $\times 10^{-1}$
4	6.250000000 $\times 10^{-2}$	-9.257812500 $\times 10^{-1}$	6.250000000 $\times 10^{-2}$	-4.687500000 $\times 10^{-2}$
5	2.031250000 $\times 10^{-1}$	-1.833007813	3.593750000 $\times 10^{-1}$	8.066406250 $\times 10^{-1}$
6	3.255208333 $\times 10^{-2}$	-2.977783203	1.542968750 $\times 10^{-1}$	1.142822266
7	-2.444118924 $\times 10^{-1}$	-4.028717041	-2.992621528 $\times 10^{-1}$	-2.324761285 $\times 10^{-2}$
8	-2.273898655 $\times 10^{-1}$	-3.409357212	-4.475063748 $\times 10^{-1}$	-2.524002923
9	1.677377960 $\times 10^{-1}$	4.411956160	-2.119700114 $\times 10^{-2}$	-3.662303224
10	4.367628576 $\times 10^{-1}$	3.284248577 $\times 10^1$	5.406151312 $\times 10^{-1}$	6.600969298 $\times 10^{-1}$
11	4.447491734 $\times 10^{-2}$	1.064643399 $\times 10^2$	4.678734733 $\times 10^{-1}$	1.029881729 $\times 10^1$
12	-6.649650688 $\times 10^{-1}$	2.537572572 $\times 10^2$	-3.650978943 $\times 10^{-1}$	3.784212529 $\times 10^1$
13	-5.647530897 $\times 10^{-1}$	4.601292420 $\times 10^2$	-9.976553176 $\times 10^{-1}$	-5.430672245
14	6.692916069 $\times 10^{-1}$	5.089128172 $\times 10^2$	-3.568290713 $\times 10^{-1}$	-4.753274080 $\times 10^1$
15	1.434455637	-4.198436299 $\times 10^2$	1.149565251	-6.050262051 $\times 10^1$
16	-7.932368314 $\times 10^{-2}$	-4.530966202 $\times 10^3$	1.548592323	3.784212529 $\times 10^1$
17	-2.535956672	-1.638065807 $\times 10^4$	-3.749497848 $\times 10^{-1}$	2.350096418 $\times 10^2$
18	-1.777648180	-4.239290399 $\times 10^4$	-2.734332838	2.710161551 $\times 10^2$
19	3.125549537	-8.305280519 $\times 10^4$	-1.897635556	-2.494277528 $\times 10^2$
n	S_3 at $k = \pi/2$	T_1 at $k = \pi/2$	T_2 at $k = \pi/2$	C_1 at $k = \pi/2$
0	2.000000000	2.000000000	2.000000000	2.000000000
1	0.000000000	-5.000000000 $\times 10^{-1}$	0.000000000	0.000000000
2	-5.000000000 $\times 10^{-1}$	-1.250000000 $\times 10^{-1}$	-6.250000000 $\times 10^{-1}$	-5.000000000 $\times 10^{-1}$
3	-2.500000000 $\times 10^{-1}$	0.000000000	-4.375000000 $\times 10^{-1}$	-2.500000000 $\times 10^{-1}$
4	-7.421875000 $\times 10^{-2}$	-3.906250000 $\times 10^{-3}$	-2.148437500 $\times 10^{-1}$	-6.250000000 $\times 10^{-2}$
5	1.123046875 $\times 10^{-2}$	-6.835937500 $\times 10^{-3}$	2.929687500 $\times 10^{-3}$	3.906250000 $\times 10^{-2}$
6	5.106608073 $\times 10^{-3}$	-5.777994792 $\times 10^{-3}$	1.789143880 $\times 10^{-1}$	4.231770833 $\times 10^{-2}$
7	-4.116566976 $\times 10^{-2}$	-8.443196615 $\times 10^{-4}$	3.243408203 $\times 10^{-1}$	-3.363715278 $\times 10^{-3}$
8	-6.972208729 $\times 10^{-2}$	-4.641285649 $\times 10^{-3}$	4.088701319 $\times 10^{-1}$	-4.214590567 $\times 10^{-2}$
9	-5.548241367 $\times 10^{-2}$	2.439375277 $\times 10^{-4}$	3.233009297 $\times 10^{-1}$	-4.348302771 $\times 10^{-2}$
10	-1.615796414 $\times 10^{-2}$	-5.090890892 $\times 10^{-3}$	-7.412812403 $\times 10^{-2}$	-1.641364313 $\times 10^{-2}$
11	1.393358333 $\times 10^{-2}$	2.287079761 $\times 10^{-3}$	-7.776608991 $\times 10^{-1}$	9.839517861 $\times 10^{-3}$
12	1.628315511 $\times 10^{-2}$	-6.726104563 $\times 10^{-3}$	-1.459665977	1.402656002 $\times 10^{-2}$
13	1.092421645 $\times 10^{-3}$	4.895928063 $\times 10^{-3}$	-1.501800181	-1.566731983 $\times 10^{-3}$
14	-7.495980128 $\times 10^{-3}$	-9.649045824 $\times 10^{-3}$	-3.338269791 $\times 10^{-1}$	-1.834857746 $\times 10^{-2}$
15	4.106539880 $\times 10^{-3}$	8.959512690 $\times 10^{-3}$	2.080412782	-2.058150001 $\times 10^{-2}$
16	2.756737781 $\times 10^{-2}$	-1.466894655 $\times 10^{-2}$	4.898068211	-8.451718109 $\times 10^{-3}$
17	4.306603014 $\times 10^{-2}$	1.550047623 $\times 10^{-2}$	6.361874618	4.993840865 $\times 10^{-3}$
18	3.910407449 $\times 10^{-2}$	-2.303464950 $\times 10^{-2}$	4.129539836	7.616721351 $\times 10^{-3}$
19	2.231265079 $\times 10^{-2}$	2.621842144 $\times 10^{-2}$	-3.760012157	-1.055977079 $\times 10^{-3}$

